Prolylpeptide Binding by the Prokaryotic SH3-like Domain of the Diphtheria Toxin Repressor: A Regulatory Switch[†,‡]

Gregory P. Wylie,[||] Vijayaraghavan Rangachari,[#] Ewa A. Bienkiewicz,[#] Vedrana Marin,[||] Nilakshee Bhattacharya,[||] John F. Love,[§] John R. Murphy,[§] and Timothy M. Logan*[,||,#,⊥]

Department of Chemistry and Biochemistry, Florida State University, Tallahassee, Florida 32306-4390, Institute of Molecular Biophysics, Kasha Laboratory for Biophysics, Florida State University, Tallahassee, Florida 32306-4380, Evans Department of Clinical Research and Department of Medicine, Boston University School of Medicine, Boston University, Boston, Massachusetts 02118, and National High Magnetic Field Laboratory, 1800 East Paul Dirac Drive, Tallahassee, Florida 32310

Received September 10, 2004; Revised Manuscript Received October 22, 2004

ABSTRACT: Diphtheria toxin repressor (DtxR) regulates the expression of iron-sensitive genes in *Corynebacterium diphtheriae*, including the diphtheria toxin gene. DtxR contains an N-terminal metal- and DNA-binding domain that is connected by a proline-rich flexible peptide segment (Pr) to a C-terminal *src* homology 3 (SH3)-like domain. We determined the solution structure of the intramolecular complex formed between the proline-rich segment and the SH3-like domain by use of NMR spectroscopy. The structure of the intramolecularly bound Pr segment differs from that seen in eukaryotic prolylpeptide−SH3 domain complexes. The prolylpeptide ligand is bound by the SH3-like domain in a deep crevice lined by aliphatic amino acid residues and passes through the binding site twice but does not adopt a polyprolyl type-II helix. NMR studies indicate that this intramolecular complex is present in the apo-state of the repressor. Isothermal equilibrium denaturation studies show that intramolecular complex formation contributes to the stability of the apo-repressor. The binding affinity of synthetic peptides to the SH3-like domain was determined using isothermal titration calorimetry. From the structure and the binding energies, we calculated the enhancement in binding energy for the intramolecular reaction and compared it to the energetics of dimerization. Together, the structural and biophysical studies suggest that the proline-rich peptide segment of DtxR functions as a switch that modulates the activation of repressor activity.

Virtually all organisms require iron for survival, although there are a few (*1*) that require Mn^{2+} rather than Fe^{2+}. In the Gram-positive bacteria, Fe^{2+} sensing and homeostasis are accomplished by a family of proteins that are homologous to the diphtheria toxin repressor (DtxR)[1] (*2*). DtxR was first shown to be the Fe^{2+}-dependent repressor that controls the expression of the diphtheria toxin in *Corynebacterium diphtheriae* (*3*) and is now known to regulate several other iron-dependent genes in this organism (*4*, *5*). DtxR is the best-characterized member of a family of over 30 related metal-activated repressors in prokaryotes (*2*) that are structurally and sequentially distinct from the Fur family of proteins (*6*, *7*). The DtxR-like repressors are frequently linked to the control of virulence factor expression because the host cells generate a growth-limiting low-iron milieu *in vivo* for the pathogen. When the bacteria's iron stores are depleted, toxins and other virulence factors are released into the surrounding environment, killing the host cells, which then release their stored iron (*7*, *8*). Thus, understanding the regulation of repressor activity in these proteins is an important starting point for developing novel strategies for controlling Fe^{2+} sensing and virulence in these pathogenic organisms.

DtxR is a 226-amino-acid, two-domain protein. The larger, N-terminal domain (residues 1−142) contains a canonical helix−turn−helix DNA-binding motif, two structurally and functionally nonequivalent metal ion binding sites, and a

[†] This work was supported by Grants 995088V to (T.M.L.) and 0225339B (V.R.) from the Florida/Puerto Rico Affiliate of the American Heart Association, AI-21628 from the Public Health Service of the National Institutes of Health (J.R.M.), and by the National High Magnetic Field Laboratory.

[‡] The coordinates and restraints lists have been deposited in the protein data bank (accession codes 1QVP and 1QW1 for SH3 and PrSH3, respectively). Resonance assignments for the two constructs have been deposited with the BioMagResBank (accession codes BMRB-6852 and BMRB-7998 for PrSH3 and SH3, respectively).

* To whom correspondence should be addressed: 502 MBB 4380, Kasha Laboratory, Florida State University, Tallahassee, FL 32306-4380. Phone: 850 644 8979. Fax 850 644 7244. E-mail: logan@sb.fsu.edu.

[||] Department of Chemistry and Biochemistry, Florida State University.

[#] Institute of Molecular Biophysics, Kasha Laboratory for Biophysics, Florida State University.

[§] Boston University.

[⊥] National High Magnetic Field Laboratory.

[1] Abbreviations: DtxR, diphtheria toxin repressor protein; SH3, construct containing residues 148−226 of DtxR, constituting the C-terminal SH3-like domain; Pr, proline-rich peptide segment of DtxR, consisting of residues 125−135; PrSH3, construct containing residues 110−226 of DtxR, constituting the Pr segment ligand and the SH3 domain receptor in a single polypeptide chain; DtxRΔSH3, construct containing residues 1−142 of DtxR, constituting the N-terminal domain plus the Pr segment; NOESY, nuclear Overhauser enhancement spectroscopy; CD, circular dichroism spectroscopy; HSQC, heteronuclear single quantum coherence spectroscopy.

10.1021/bi048035p CCC: $30.25
Published on Web 12/08/2004

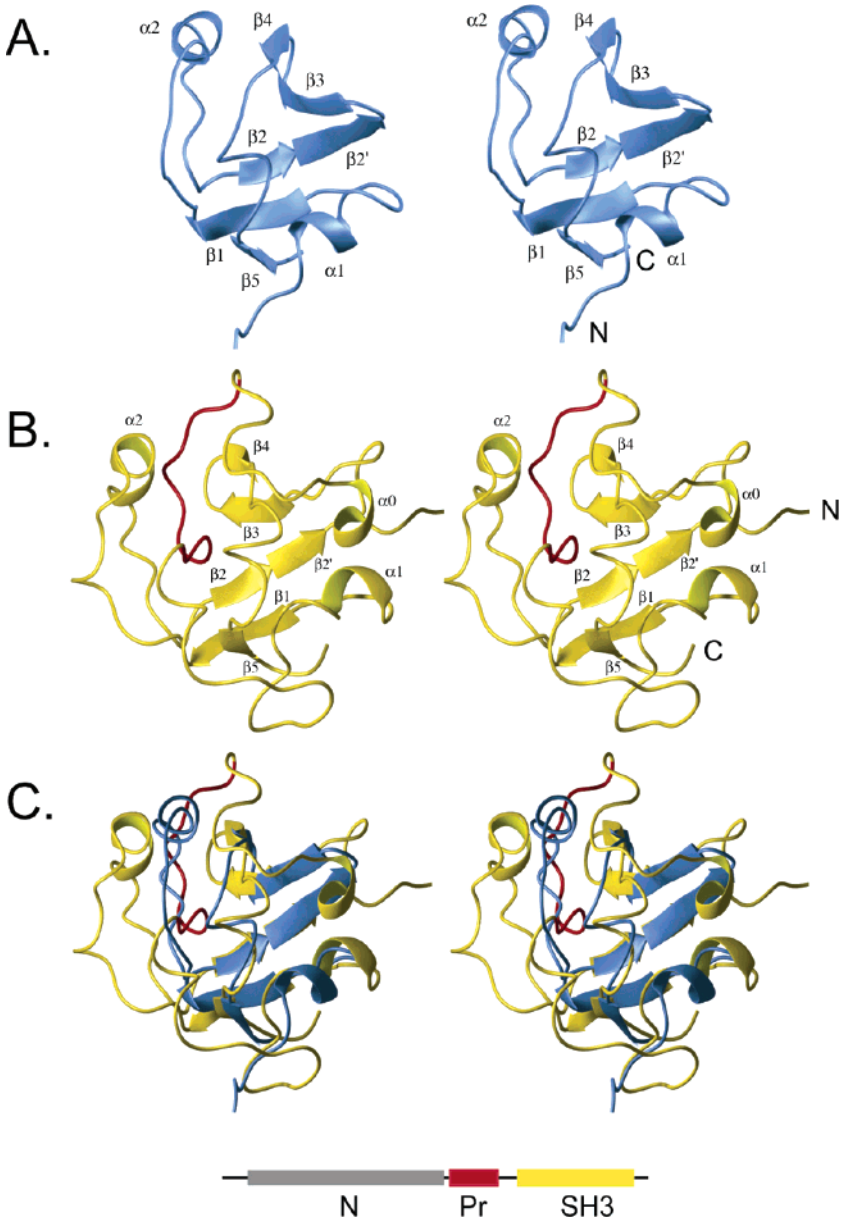

FIGURE 1: Structure of SH3 and PrSH3 from the diphtheria toxin repressor. (A) Side-by-side stereo ribbon diagram of the minimized average structure of the unbound SH3-like domain from DtxR. (B) Side-by-side stereo ribbon diagram of the average structure of PrSH3 intramolecular complex. The orientation is identical to that of the SH3 domain shown in panel A. The schematic diagram at the bottom of the figure shows the organization of the DtxR structural gene, indicating the relationship of the N, Pr segment and SH3 domains. The Pr segment and SH3 domain are color-coded to match the structure shown in panel B of this figure. (C) Superposition of the SH3 and PrSH3 structures. All figures were generated in Molmol (*64*) and rendered in POV Ray (http://www.povray.org).

dimerization interface (*9*, *10*). The C-terminal domain (residues A148−L226) is structurally homologous to eukaryotic SH3 domains (*11*−*13*) and is separated from the N-terminal domain by a short, flexible proline-rich peptide segment. The physiological ligand is Fe^{2+}, although, to varying degrees, DtxR binds and is activated by a range of divalent transition metals in vitro (*14*), including Mn^{2+}, Co^{2+}, Ni^{2+}, Zn^{2+}, and Cd^{2+}. The metal-binding site formed by residues M10, C102, E105, and H106 (the primary site) is required for the repressor activity, whereas the metal site formed by residues H79, E83, and H98 (the ancillary site) is not (*15*). Residues E170 and Q173 in the SH3-like domain complete the coordination sphere of the ancillary site in Co^{2+}-activated DtxR (*12*). A similar interaction is seen in the structure of the DtxR homologue from *Mycobacterium tuberculosis*, IdeR (*16*). The biological importance of this interdomain coordination in repressor function was recently established in DtxR (*17*).

The molecular steps involved in activation of repressor activity in DtxR by metal ions are poorly understood. In the absence of metal, the entire N-terminal domain exists as an ensemble of partially ordered conformers in solution, resembling a molten globule (*18*). Binding divalent transition metals triggers a disordered-to-ordered structural transition in this domain that increases the affinity for the dimeric state (*19*) and activates DtxR for sequence-specific DNA binding. Previous solution NMR studies demonstrated a binding interaction between the proline-rich peptide segment (residues R125−G139; referred to as Pr) and the SH3 domain (A148−L226) (*13*). This intramolecular SH3−Pr binding interaction may regulate the activity of the N-terminal domain in a manner analogous to that found in eukaryotic receptor

tyrosine kinases (*20*, *21*). Here, we investigate the structural basis for prolylpeptide binding by this prokaryotic SH3 domain by determining the solution structure of the SH3 domain bound to the Pr segment in an intramolecular complex (residues D110−L226; referred to as PrSH3). We also show that this structure is present in apo-DtxR and that it contributes to the observed stability of the N-terminal domain.

RESULTS

Residues A148−L226 Form an Unusual SH3-like Domain. Previous structural studies of the C-terminal domain from DtxR contained a portion of the Pr segment (residues N130−G139) that was preceded by a hexa-histidine tag, which lead to oligomer formation in solution (*13*). To more fully explore ligand recognition and binding in this domain, the partial Pr segment and the affinity tag portion were removed and, starting from residue D144, the structure of this construct was solved. The structure of the SH3 domain consists of six β-strands that form two partially orthogonal antiparallel β-sheets that are connected by two long loops (Figure 1a). The first β-sheet is composed of strands β1 (V163−Q167), β5 (I221−E224), and β2 (E192−V193), which is shared by both β-sheets. The second β-sheet is composed of strands β2′ (E194−R198), β3 (H201−H206), and β4 (K209−L213). A single-turn 3_{10} helix (α1; residues V152-A155) precedes β1. A long loop containing an α-helix (α2; residues Q178−D184) connects strands β1 and β2. Strands β4 and β5 are connected by a short loop of nonregular secondary structure. Interestingly, the hydrophobic core is formed almost entirely by the side chains of aliphatic residues V152, A155, A156, V163, I165, L182, A185, I187, V193, I195, L204, V211, L213, L217, A218, I221, and I223. There are no tyrosine or tryptophan residues in the SH3 domain, and, of the two phenylalanines, only F179 participates in the hydrophobic core.

Residues D110−L226 Form a Monomeric, Intramolecular Complex. The PrSH3 construct is monomeric in solution, as demonstrated using several different and complementary experiments. First, there was essentially no change in the ^{1}H and ^{15}N resonance frequency of backbone amides for residues involved in ligand binding over a 10-fold concentration range (100 μM to 1 mM; see Supporting Information Figure 1). Second, no NOEs were detected in ω_1-^{13}C half-filtered NOESY spectra (*22*) collected on an equimolar mixture of ^{13}C-labeled and unlabeled PrSH3 (not shown). Third, PrSH3 migrated as a single band on native polyacrylamide gels with an apparent molecular weight consistent with monomeric protein, and fourth, the self-diffusion coefficient measured by NMR spectroscopy (*23*) on a 1 mM sample was 1.06×10^{-6} cm^2/s (not shown). This corresponds to a hydrated molecular mass of 16.4 kDa, which is in good agreement with the predicted (unhydrated) mass of 15.3 kDa. These results, together with the structural data, indicate that the PrSH3 construct forms an intramolecular complex.

Structure of the Intramolecular Complex. The overall architecture of PrSH3 is similar to that of the unligated SH3 domain (Figure 1b). Both contain five β-strands with an α-helix (residues T180−D184) in the loop connecting β1 and β2. The differences between the "bound" and "unbound" states are that (1) the short β-strand and single-turn helix seen in residues V152−A155 of the SH3 domain are not formed in PrSH3, and (2) a helical turn is seen for residues A155−T157 in PrSH3 that is not observed in SH3. These changes are presumably due to restrictions placed on the backbone conformation to accommodate binding of the Pr segment. The β-strands of the bound structure superimpose on the unbound structure with 0.87 Å root-mean-square (rms) deviation for the backbone heavy atoms, indicating that ligand binding does not alter the core of the structure. In contrast to the β-sheets, helix α2 is moved away from the protein core by 5.3 Å to accommodate the ligand, which occupies approximately the same place as α2 in the uncomplexed protein (Figure 1c). Finally, the rms deviation of the backbone atoms in the 13 lowest energy structures is higher for PrSH3 than for the uncomplexed domain (Table 1).

Table 1: Structure Statistics

	SH3	PrSH3
NOE restraints		
total	1167	1325
intraresidue	529	780
medium range	49	280
long range	128	265
ϕ angle restraints	34	79
hydrogen bond restraints	29	29
average energies (kcal/mol)		
total	137 ± 13	240 ± 25
NOE	9 ± 2	22 ± 4
bonds	3 ± 1	8 ± 1
angles	33 ± 3	56 ± 7
improper	3 ± 1	5 ± 2
VDW	87 ± 7	147 ± 14
Ramachandran plot		
most favored	63	59
allowed	28	29
generously allowed	6	9
backbone rmsd (Å)		
residues 147−226	1.67 ± 0.37	1.24 ± 0.50
all β-strands	0.70 ± 0.15	0.60 ± 0.31

The proline-rich peptide segment (residues R125−G139; RSPFGNPIPGLDELG) does not form the left-handed polyprolyl type II (PPII) helix seen in ligands of eukaryotic SH3 domains; instead the prolylpeptide region adopts an extended conformation when bound to the SH3-like domain (Figures 1b and 2a). It is unlikely that this unusual bound conformation reflects an inherent limitation in the ability of this peptide to adopt a left-handed PPII helical conformation. PPII helix formation is not restricted to proline-rich peptide sequences; peptides that lack prolines can form PPII helices (*24*). Indeed, the intramolecular proline-containing peptide ligands for Src and other receptor tyrosine kinases contain a single proline residue, yet they form PPII helices when intramolecularly bound to their SH3 domains (*20*, *21*). Synthetic peptides corresponding to the Pr segment of DtxR adopt a conformation that is consistent with the PPII helical structure in solution based on their far-UV CD spectra (data not shown). Therefore, bound conformation adopted by the Pr segment results from specific interactions with the SH3-like domain.

The peptide ligand is buried in the hydrophobic core of the protein (Figure 1b). The ligand enters into the binding pocket, turns nearly 180° to make contacts within the binding pocket of the SH3 domain, and then forms additional contacts with the SH3 domain away from the primary binding pocket. The proline residues P131 and P133 each make multiple contacts with the side chains of aliphatic residues within the

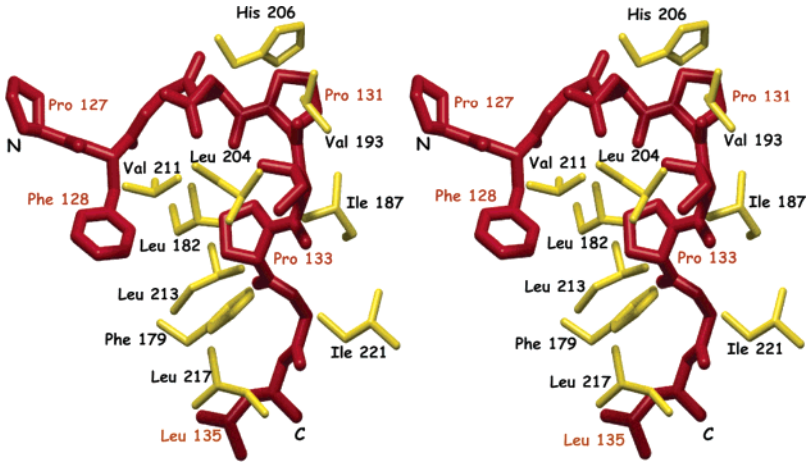

FIGURE 2: The Pr segment binding pocket in the DtxR SH3-like domain, shown in side-by-side stereo. Backbone and the side chain bonds of the ligand residues (P127−L135) are shown in red, while the side chain bonds of residues from the SH3-like domain that form contacts with the ligand are indicated in gold.

hydrophobic core of the SH3-like domain (Figure 2). P133 is contacted by residues L182, I187, V211, L217, and I221, while P131 interacts with V193 and H206. The side chain of residue L204 is packed between the P131 and P133 side chains. The additional contacts between the ligand and the SH3-like domain involve the methyl groups of residues V112 and V152, I153, A156, and I202. There is an apparent Coulombic interaction between the side chains of R125 and D210 and E212, which constitute a patch of negative potential at the top of the binding site. This interaction may be analogous to the interaction between the Arg side chain and a conserved acidic side chain in the RT loop observed in complexes of high-affinity prolyl-peptides and eukaryotic SH3 domains that orients the ligand to bind in one of two binding configurations (*25*).

Ligand Binding Energetics. To explore the validity of the structural model derived from the NMR data, we investigated the intermolecular ligand binding energetics of synthetic peptides binding to the SH3 domain construct using isothermal titration calorimetry (ITC). Synthetic peptides corresponding to the proline-rich peptide segment (residues R125−G139) were added to a solution containing the unliganded SH3 domain, and the temporal heat evolution was measured. A typical titration for the wild-type peptide, p1, is shown in Figure 3a. The data show an initially weak exothermic binding that increases in magnitude (becomes more exothermic) with increasing ligand concentration. Separate control experiments showed large exothermic heats associated with titration of the peptide into phosphate buffer in the absence of SH3, which suggested that the peptide was aggregating in the highly concentrated stock solution (see Methods). Far-UV circular dichroism studies indicated a concentration-dependent change in peptide structure. Plots of the molar ellipticity at 210 nm as a function of peptide concentration indicated self-association (*26*) of varying orders for the different peptides investigated (data not shown). Furthermore, binding experiments performed in Tris buffer revealed that peptide binding was also linked to changes in the protonation of one or more ionizable groups (*27*), possibly that of H206. Due to the complications associated with deriving exact thermodynamic quantities for binding in the presence of ligand aggregation and proton linkage, we adopted a phenomenological approach of fitting the observed heats of dilution of the peptide to a second-order polynomial and used this to correct the raw peptide binding data (*28*, *29*). The corrected binding isotherms (Figure 3b) were fit to the single-site Wiseman isotherm (*30*), yielding an apparent equilibrium dissociation constant of 740 (±30) μM and an apparent enthalpy of binding (ΔH^{app}) of −1.13 (±0.02) kcal/mol at 25 °C. Mutating any of the prolines in the synthetic peptide to alanine essentially abrogates binding (Table 2). There was no binding to proline-rich synthetic peptides known to adopt a left-handed PPII helical structure in complex with eukaryotic SH3 domains (peptide sequence: RPFGPPLP and PFGPPLPPR; data not shown).

Proline Mutants Still Form the Intramolecular Complex. The Pro → Ala mutants had a less dramatic effect on formation of the intramolecular complex when introduced into the PrSH3 construct than was observed with the synthetic peptides, although the results are qualitatively consistent with the intermolecular binding study. Specifically, mutating the proline residues to alanine resulted in modest changes to the backbone ^{1}H and ^{15}N chemical shifts of the residues lining the binding pocket (Figure 4). The P127A and P131A mutants had a relatively modest effect on binding, whereas the P133A mutant was more perturbing. A mutant in which V211 and L213 in the SH3 domain were simultaneously mutated to Ala failed to adopt a folded structure.

PrSH3 Structure Models the Interdomain Interactions in ApoDtxR. We investigated whether the SH3 domain formed an intramolecular complex with the Pr segment in full-length apoDtxR by comparing the resonance frequency of backbone ^{1}H and ^{15}N resonances observed in high-resolution HSQC spectra of apoDtxR, PrSH3, and SH3. If the intramolecular complex was formed in apoDtxR, we reasoned that the resonances of PrSH3 would be similar to that of the SH3 domain resonances of apoDtxR. If the complex was not present, or if there were other domain−domain interactions, then the SH3 domain resonances of apoDtxR would resemble the resonances of SH3 domain or be different from both SH3 and PrSH3. Figure 5 shows the chemical shift difference ($\Delta\delta$) for SH3 domain resonances of apoDtxR compared to these two constructs. As shown in the figure, there are large $\Delta\delta$ values observed between apoDtxR and SH3. The average $\Delta\delta$ value was 18 Hz (digital resolution = 7 Hz), and ~30% of all resonances were similar within the digital resolution

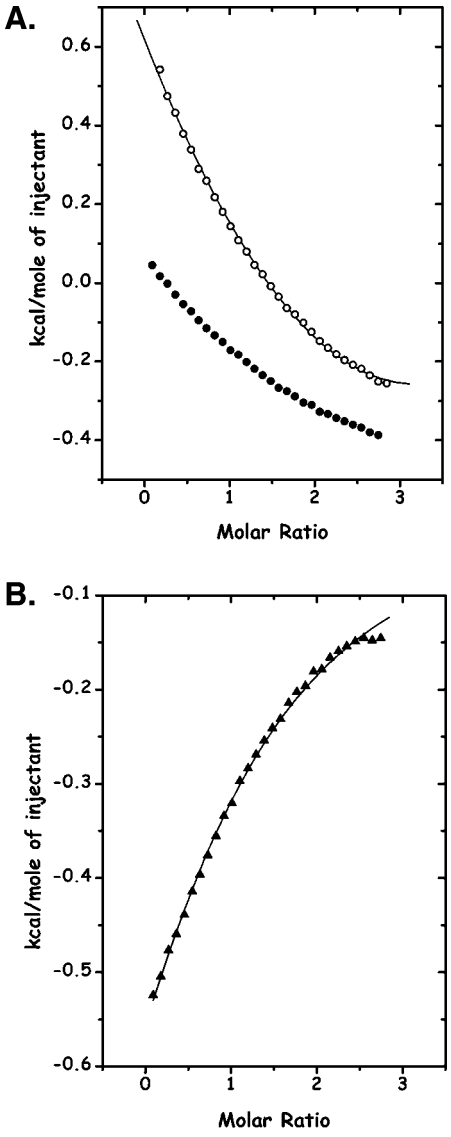

FIGURE 3: Isothermal titration calorimetry of p1 peptide binding to the SH3-like domain. (A) Integrated heats obtained upon addition of peptide p1 to SH3 (solid circles) and to buffer (open circles). The buffer heats were fit to a second-order polynomial (solid line) that characterizes the concentration dependence of diluting the peptide into the calorimetry cell. (B) Integrated heats evolved for titration of p1 peptide, corrected for the heats of peptide dilution. The corrected data are fit to the single-site binding isotherm defined by Wiseman (*30*) (solid line).

Table 2: Thermodynamics of Prolylpeptide Binding to SH3[a]

Peptide	Sequence	K_d^{app}, μM	ΔH^{app}, kcal/mol	ΔS^{app}, cal/mol.K
p1	RSPFGNPIPGL	740 ± 20	-1.13 ± 0.02	10.50 ± 0.02
p2	**A**********	2300 ± 20	-0.90 ± 0.02	9.10 ± 0.01
p3	*******A*****	-ND-[†]	--	--
p4	**********A**	-ND-[†]	--	--

[a,†] ND: no binding detected under conditions used for the titration. This indicates that the equilibrium dissociation constant is greater than 3 mM. All experiments were performed at 25 °C.

of the two spectra. On the other hand, the $\Delta\delta$ values for apoDtxR and PrSH3 were smaller (average $\Delta\delta$ value = 11 Hz with >60% of the resonances similar within digital resolution). Similar chemical shift changes were observed by introducing DtxRΔSH3 to ^{15}N-labeled SH3 (not shown). These results suggest the presence of interdomain interactions

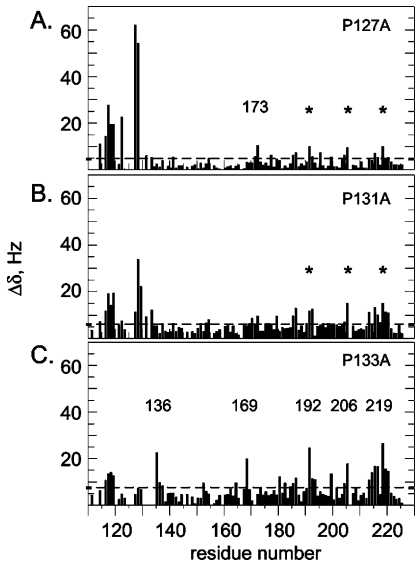

FIGURE 4: Chemical shift difference plots comparing the effect of Pro → Ala mutations in the PrSH3 complex. (A) P127A, (B) P131A, and (C) P133A. The shift differences ($\Delta\delta$) were calculated as described in Materials and Methods. The horizontal dashed line indicates the limit of the digital resolution for each spectrum. Residues exhibiting large changes in backbone chemical shift in P133A include D136, N169, E192, H206, and H219. These latter three residues are indicated by asterisks in P131A and P127A. Q173 is also indicated in P127A.

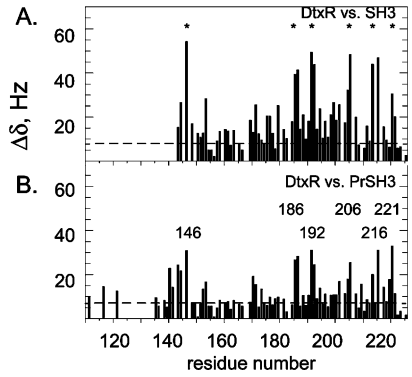

FIGURE 5: Chemical shift difference plots comparing the SH3 resonances in the full-length wild-type protein to that of the SH3 (A) and PrSH3 (B) constructs. The shift differences ($\Delta\delta$) were calculated as described in Materials and Methods. The horizontal dashed line indicates the limit of the digital resolution for each spectrum. The residues exhibiting the largest change in chemical shift in PrSH3 are indicated by A146, D186, E192, H206, D216, and I221. These same residues are indicated by an asterisk in the plot for SH3.

between the two domains of apoDtxR in solution. Furthermore, the similarity in the SH3 domain chemical shifts suggests that the PrSH3 structure determined here is a good model for these interactions.

Interdomain Contacts Contribute to the Stability ApoDtxR. The significance of the intramolecular interdomain contacts between the SH3 domain and the N domain was investigated by measuring isothermal equilibrium denaturation profiles of wild-type full-length protein and several mutants. DtxR contains a single tryptophan (W104) that is near the primary metal-binding site and at the dimerization interface. The integrated fluorescence intensity of W104 was measured as a function of increasing urea concentration and transformed into the fraction unfolded (Figure 6). ApoDtxR exhibits a linear change in fluorescence that plateaus at ~1.5 M urea.

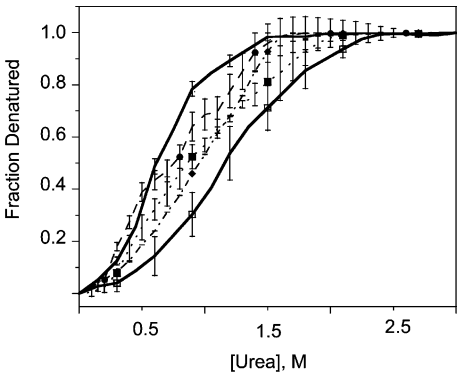

FIGURE 6: Isothermal denaturation profiles for wild-type and four mutant constructs of apoDtxR. The data represent the averages of a minimum of two independent determinations. Symbols: The solid lines are for wild-type (○) and DtxRΔSH3 (□); dashed lines are for P127A (●), P131A (■), and P133A (▲).

Table 3: Repressor Activity in DtxR Mutants

construct	activity[a]
wild-type	0.13 ± 0.02
P127A	34.0 ± 2.4
P131A	1.8 ± 0.1
P133A	35.6 ± 5.2
DtxRΔSH3	24.4 ± 2.8
Q173A/E170A	9.6 ± 1.0

[a] Activity reported as percent of control β-galactosidase activity determined in a strain carrying a plasmid that lacks the DtxR structural gene.

In the absence of stable tertiary structure in the apo-protein, there is no pretransition baseline. In contrast, the denaturation profile for metal-activated DtxR exhibits an extended pretransition region with a denaturation midpoint of ∼5 M urea (V. Marin and T. Logan, unpublished). The denaturation profile for apoDtxR is clearly not two-state. A semiquantitative comparison of the isothermal denaturation profiles of several mutants was made by determining the urea concentration at the midpoint of the profile. Figure 6 also shows the isothermal denaturation profile of the apo form of DtxRΔSH3 (residues M1−N142), which lacks the SH3 domain. In contrast to the full-length apoDtxR, the denaturation profile of DtxRΔSH3 exhibits a slight pretransition baseline with a denaturation midpoint of ∼1.15 M urea, compared to 0.6 M for the wild-type protein. The increased stability of DtxRΔSH3 is consistent with a higher fraction of dimer found for this protein in native gel electrophoresis experiments and the greater number of dispersed resonances of HSQC spectra compared to DtxR (data not shown). The denaturation profiles for the three Pro → Ala mutants are shown in Figure 6. Although there is some scatter associated with the profiles, the midpoint of the denaturation profiles of P127A, P131A, and P133A (0.75, 0.85, and 0.95) is bracketed by those of full-length and DtxRΔSH3.

An Intact Pr Segment Is Required for Repressor Function. Repressor activity was measured using an in vivo assay in which the expression of β-galactosidase is under the control of a hybrid *tacPtoxO* promoter/operator (*31*). Metal-activated DtxR represses expression of β-galactosidase, although this repression can be relieved by the addition of the transition metal ion chelator 2,2′-dipyridyl to the growth medium (*31*). As summarized in Table 3, wild-type DtxR is able to repress completely the expression of β-galactosidase. In contrast, there is reduced repressor activity when either P127 or P133 is mutated to alanine. The P131A mutation had minimal effects on repressor activity. DtxRΔSH3 was substantially less active than either wild-type DtxR or DtxR(E170A,-Q173A).

DISCUSSION

Comparison to Eukaryotic Prolylpeptide-Binding Domains. Prolylpeptide binding is an essential component of many signal transduction and macromolecular assembly pathways in eukaryotes, and a number of modular domains, including SH3 domains, have evolved to accomplish this task. Although these various domains have unrelated amino acid sequences and adopt different structures, they exhibit common features that are involved in prolylpeptide binding. First, the peptide binding surface is formed by conserved aromatic amino acid side chains that pack against and make specific contacts with the prolylpeptide ligand, including hydrogen bond formation with backbone carbonyl groups in the ligand. In SH3 domains, the hydrogen bond donor is typically the indole hydrogen of a conserved tryptophan residue (*25*). Second, the ligand adopts a left-handed polyproline type II (PPII) helix, which is capable of forming similar contacts with the binding pocket whether it is bound in an N → C or C → N orientation. The binding orientation adopted by individual peptides is determined by electrostatic interactions between ligand residues flanking the PPII helix and protein residues located in flexible loops positioned on either side of the binding pocket (*32*). SH3 domains bind peptide ligands with a relatively high specificity and moderate binding affinity (equilibrium dissociation constants in the range of 1−100 μM) (*33*). Furthermore, binding specificity and affinity is enhanced through interactions with residues adjacent to the PPII helix in the three-dimensional structure of the ligand (*25*). Indeed, SH3 domains can bind "noncanonical ligands" in the same binding site as that of high-affinity canonical ligands (*20*, *34*−*38*), indicating that the binding site in the SH3 domain fold can accommodate a range of sequences and structural interactions.

Prokaryotic signaling pathways are based on a set of modular proteins that is essentially nonoverlapping with those found in eukaryotes (*39*). Of the few examples of SH3-like domains identified in prokaryotic organisms (*40*, *41*), none have been demonstrated to bind proline-rich peptides or to participate in signal transduction. Therefore, it is interesting to compare ligand binding by the prokaryotic DtxR SH3 domain to the eukaryotic SH3 domains. The ligand is bound in a similar topological region, namely, between the β-sandwich structure and the loop connecting strands β2 and β3, but the conformation of the bound ligand and the chemical nature of the binding pocket differ considerably from that of eukaryotic SH3 domains. The most obvious difference is that the ligand does not form a PPII helical structure when bound to the protein surface. Instead, the ligand adopts a more extended conformation and is buried in the hydrophobic core of the domain. The proline residues may serve to kink the chain into a hairpin-like conformation that allows additional contacts with the SH3-like domain. The SH3 domain from BP53 also binds its ligand, the L3 loop of ankyrin, in a hairpin conformation, but the ligand binds to the surface of the SH3 domain (*36*) rather than in the hydrophobic core. The binding mode seen in the DtxR SH3

domain requires large structural changes to accommodate the ligand, in contrast to the small structural changes observed in prolylpeptide binding by eukaryotic SH3 domains (*42*).

The novel binding mode of the DtxR SH3 domain is also reflected in the energetics of ligand binding. The DtxR SH3 domain binds a synthetic peptide corresponding to its natural ligand with only modest affinity (~740 μM) compared to the affinity of eukaryotic SH3 domains for optimized polyproline ligands (~1−100 μM (*33*)). Additional binding interactions between the ligand and residues outside of the binding pocket are observed in Hck SH3 domain that serve to substantially enhance affinity and specificity (*43*). A similar situation exists in the DtxR SH3 domain, where the ligand makes two passes through the binding site, and then makes additional contacts away from the binding site. These additional contacts may contribute to binding affinity in the native construct, as we observe enhanced binding between the SH3 domain and DtxRΔSH3 (K_d ~ 1.5 μM; V. Marin and T. Logan, unpublished). The identification of chemical shift differences between full-length DtxR and PrSH3 further suggests that additional interactions are occurring in the native protein that are not completely identified in this simplified model system.

The DtxR ligand binding pocket is composed almost entirely of aliphatic hydrophobic groups rather than aromatic amino acids found in eukaryotic SH3 domains and in other PPII-binding domains. Aliphatic amino acids are less polar than aromatic amino acids. Consequently, the thermodynamics of binding by the prokaryotic SH3 domain are different than that of eukaryotic SH3 domains. For peptides that readily adopt a PPII helical structure in solution, binding to eukaryotic SH3 domains is enthalpically driven and is unfavorable entropically (*44*, *45*). The favorable enthalpy of binding in eukaryotic SH3 domains reflects (1) the participation of a conserved Coulombic interaction between an Arg residue on the ligand and an acidic group on the RT loop of the SH3 domain, and (2) the higher polarity of aromatic as compared to aliphatic amino acid side chains (*46*). Recently, however, it has been pointed out that PPII helix formation upon binding substantially contributes to the energetics and that binding peptides already in the PPII conformation may be entropically driven (*47*). In contrast, the DtxR SH3 domain does not bind a peptide that adopts a PPII helical structure and binds the internal proline-rich peptide segment with favorable ΔS^{app} and neutral ΔH^{app} (Table 3). The ΔS^{app} of binding by the DtxR SH3 domain indicates changes in the ligand configurational entropy, as well as the greater release of waters from the large nonpolar surface of the aliphatic binding pocket than is observed in the eukaryotic domain.

The observed intermolecular peptide binding affinity measured for the DtxR SH3 domain is similar in magnitude to that observed for intermolecular binding in the Tec kinase SH3 domain (*38*). The weak intermolecular binding in Tec kinase is substantially enhanced in the intramolecular complex, and a similar effect is observed for the PrSH3 complex of DtxR. While it is possible that the intermolecular ligand may bind in a manner that differs from that of the intramolecular ligand in both of these proteins, it is more likely that the weak intermolecular binding observed for model peptides reflects a fine-tuning of the actual intramolecular binding affinity to a level that effectively competes with other physiological binding processes. Since the intermolecular binding of the Pr segment is quite modest, we estimated the effective concentration of the Pr segment for intramolecular binding by the SH3 domain by modeling the intervening loop of amino acid residues as a wormlike chain (*48*). Taking the distance between the Cα atom positions of residues L138−A148 as the endpoints of the loop (17.7 Å) and 3.04 Å as the distance between Cα atoms of adjacent monomers in this chain (*48*) yields an effective concentration of 23 mM for the Pr segment. In practical terms, this enhances the fraction bound by a factor of 1.70 over intermolecular binding of the same ligand at 1 mM free concentration. Put another way, the intramolecular nature of the binding reaction lowers the apparent equilibrium dissociation constant of the Pr segment from the SH3 domain to approximately 32 μM, which is in a range to effectively compete with activation by metal ions.

The intramolecular enhancement also provides an explanation for the apparently larger effect of the Pro → Ala mutants in the intermolecular peptide binding experiments relative to that of the intramolecular complex formation experiments. The intermolecular peptide binding experiments indicate a substantial change upon substituting Ala for either of the Pro residues, whereas the effects are minimal when the mutations are introduced into the PrSH3 complex. Using the parameters above, changing the binding affinity by a factor of 2 for the synthetic peptides (as seen in the p2 peptide) decreases the fraction bound of from 60% to less than 30%, which is beyond the sensitivity of the ITC experiment. In contrast, changing the affinity by a factor of 2 for the P127A PrSH3 mutant decreases the fraction bound from 97 to 75%, resulting in a relatively modest change in the observed backbone chemical shifts compared to the wild-type PrSH3 construct.

Insight into DtxR Regulation. The molecular mechanism(s) by which metal binding activates repressor activity in DtxR and its homologues is unknown, in large part because the disordered structure of the apo-repressor has frustrated detailed structural characterization of this state. This study clearly points to the SH3 domain of DtxR as playing an important role in this process.

In the holo-repressor, the SH3-like domain contributes two coordinating ligands to the ancillary metal-binding site. Recent studies indicate that coordination of metal in the ancillary site by the side chains of the residues E170 and Q173 in the SH3-like domain is required for full repressor activity (*17*). The decreased repressor activity of DtxRΔSH3 reported here confirms and extends these observations. The results presented here also indicate the importance of an intact Pr segment for repressor activity. P127 and P133 make significant stabilizing contacts with the N domain, and, in particular, interact with the residues in and near the ancillary binding site in the active, holo-repressor. P131, on the other hand, is directed away from the N domain (*12*). Repressor activity is reduced in the P127A and P133A mutants relative to wild-type, whereas the P131A mutant is essentially the same as wild-type. Thus, the repressor assay data report on the structural and functional integrity of the activated state and not on the interactions present in the inactive apo-repressor that are modeled by the PrSH3 structure. In contrast, the intermolecular peptide binding studies and the effects of the Pro → Ala mutants on the PrSH3 chemical

shifts reflect interactions that occur in the apo-repressor and can be interpreted from the PrSH3 structure.

The structure of the PrSH3 intramolecular complex demonstrates that domain−domain interactions are present in apoDtxR, and that these interactions are different from those seen in the holo-protein. The intramolecular binding of Pr segment by the SH3-like domain may contribute to repressor activation. The Pr segment binds to the back of the three helices in the N domain that form the dimer interface (*9*, *10*), making numerous hydrophobic contacts and stabilizing the active form of the repressor. If these stabilizing interactions were diminished due to competitive binding of the Pr segment between the N and SH3 domains in the apo-repressor, then the N domain would be destabilized, possibly to the point of molten globule formation, as observed in solution for the apo-protein (*18*). The intramolecular binding between the SH3 domain and the Pr segment has not been observed in crystal structures of apo DtxR because the process of crystallization biases the conformational averaging toward more compact states that resemble the conformation of the active repressor. On the other hand, the backbone N and HN chemical shifts of the SH3-like domain in full-length DtxR differ considerably from those of the free SH3 domain and more closely resemble those of the intramolecular complex. By complexing the Pr segment in the apo-state of the repressor, the SH3-like domain would increase the barrier for forming the activated state, altering the inactive−active equilibrium toward the inactive state. From a simple competitive binding model, we estimate that this intramolecular binding may increase the concentration of inactive form by an order of magnitude, dramatically affecting repression by DtxR.

Intramolecular binding of the Pr segment may also serve to localize the SH3-like domain in a conformation to preform the ancillary metal-binding site. By binding to the Pr segment, the SH3 domain is localized near the residues forming the ancillary site, effectively increasing the affinity of E170 and Q173 for coordination of the metal. In the metal bound form, the Pr segment backbone adopts a substantially different conformation from that seen in the PrSH3 complex (Figure 7). The side chains of Ser126 and Asn130 stabilize the active state of the repressor (*49*); in PrSH3 the side chains of these residues are oriented in the opposite direction and could not form the same interactions as seen in active DtxR. This conformational change essentially prevents the simultaneous binding of the Pr segment by the N and SH3 domains. Thus, the Pr segment dissociates from the SH3-like domain and binds tightly to the N domain, stabilizing the active dimer form of the repressor.

A schematic model for DtxR activation that incorporates these ideas is shown in Figure 8. In the weakly dimeric apo-repressor, the SH3-like domain binds to the Pr segment and the N domain adopts a partially ordered, molten globule conformational ensemble (*18*). Because of restraints imposed by the backbone geometry of the residues that tether the two domains, the SH3-like domain is constrained to be close to the N domain. Upon activation by divalent transition metal ions, the N domain folds into a more ordered conformation and increases its affinity for dimerization (for clarity, the dimerization step is not shown in the figure). In this state, the SH3-like domain is dissociated from the Pr segment and helps to coordinate the ancillary metal.

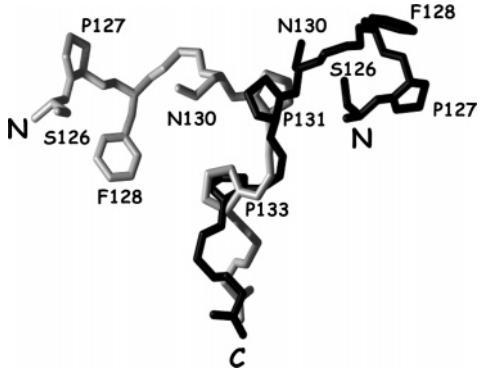

FIGURE 7: Superposition of the Pr segment in the active (light gray) and inactive (dark gray) states of DtxR. The structure of the Pr segment in the active state is the crystal structure of Co^{2+}-activated DtxR (1c0w); the structure in the inactive state is from the NMR structure presented here. The side chains of residues P127, F128, N130, P131, and P133 are indicated. When the backbone atoms of these residues are superimposed and fixed with respect to each other, it is apparent that the C-terminal portion of the Pr segment adopts relatively similar conformations in the active and inactive states, whereas the conformation of the N-terminal part of the Pr segment changes by approximately 180°. This is due primarily to changes in the ψ angle of residues G129 (76.1° active state; −149.7° inactive state) and I132 (−67.0° active state; 148.9° inactive state). The changes in these backbone angles effect a substantial movement of the Ser126 and Asn130 side chains from the inactive to the active form of the repressor.

The equilibrium constant(s) for binding divalent transition metal ions by DtxR has not yet been accurately determined, but is thought to be in the low micromolar range (*19*), which compares favorably with the amount of free Fe^{2+} in vivo (*50*). Using these parameters, the intramolecular binding of Pr segment by the SH3 domain can compete favorably with this binding to yield effective regulation of DtxR. Thus, it appears that the Pr segment functions as a molecular switch that aids in converting the inactive to the active repressor. When the Pr segment is bound to the SH3 domain, the repressor is in the "off" state, whereas when the Pr segment and metal ions are bound to the N domain, the repressor is switched "on". The high sequence homology between DtxR and its homologues suggests that a similar regulatory scheme operates in these related proteins, as well.

MATERIALS AND METHODS

Protein Expression and Purification. Expression and purification of the SH3 domain was performed as described previously (*13*). The gene for the PrSH3 construct was generated via the polymerase chain reaction using a forward primer (5′-ATTATTCATATGGACGAAGTTGAACGCAG-GC-3′) that coded for an *Nde*I restriction site and residues D110 to R115 of intact DtxR, which was used as the template. The reverse primer (5′-AATGGATCCTCATTA-GAGTTCTTCGATACG-3′) contained nucleotides coding for residues I223−L226 of DtxR, two stop codons, and a *Bam*HI site. The doubly digested PCR product was ligated into similarly digested pET-15b plasmid (Novagen, Madison, WI) and transformed into BL21(DE3) cells for protein expression.

Uniformly labeled samples of $^{15}N/^{13}C$ of SH3 and PrSH3 were expressed in BL21(DE3) grown in M9 minimal medium containing 1 g/L of $^{15}NH_4Cl$ and 2 g/L [U-$^{13}C_6$]-glucose, induced with isopropylthiogalactoside (final con-

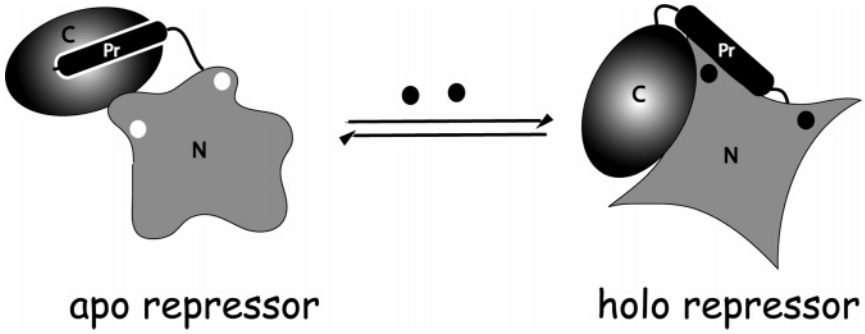

FIGURE 8: Schematic diagram indicating the role of interactions between the SH3-like domain and the Pr segment during the activation of DtxR. In State 1, the Pr segment is bound by the SH3-like domain in a structure that resembles that determined in this work. This state may function to localize the SH3 domain in a conformation that favors subsequent metal binding to the ancillary site and/or it may serve to minimize binding of the Pr segment to the N domain, effectively increasing the concentration of the inactive repressor. Metal binding (represented by the solid circles) effects a disordered-to-ordered conformational change in the N domain. During this transition, the SH3-like domain dissociates from the Pr segment and coordinates the ancillary metal. In the active state of the repressor, the Pr segment is bound by the N domain.

centration ~0.4 mM) and harvested by centrifugation. The cell pellet was resuspended in binding buffer (50 mM potassium phosphate containing 5 mM imidazole, 0.5 M NaCl, pH 7.5) and lysed by passage through a high-pressure cell. The debris was pelleted, and the supernatant was applied to an immobilized metal affinity column, which was pre-equilibrated in five column volumes of binding buffer. Protein was eluted by using 50 mM potassium phosphate containing 0.50 M NaCl and 0.50 M imidazole at pH 7.5. The pH was lowered to 6.5 for fractions containing recombinant protein, and the histidine tag was removed by digestion with thrombin (0.1 U per 1 mg of protein) at room temperature for 16 h, or for 4 h at 37 °C in a dialysis membrane (6000 molecular weight cutoff) to allow separation of the cleaved histidine tag. The digestion reaction was stopped by addition of phenylmethylsulfonyl chloride, ethylenediamine tetraacetate, and ethyleneglycol tetraacetate each at 100 μM final concentration. In some cases, the excess thrombin was removed by use of cation exchange chromatography (CM-52) in the 50 mM (10 mM) potassium phosphate, pH 6.5, for SH3 (PrSH3). Both SH3 and PrSH3 eluted in the flow-through. The cleaved protein was concentrated to 1−2 mM. Protein concentration was determined using the Coomassie Plus Protein Assay reagent (Pierce Chemical Co., Rockford, IL) using bovine serum albumin as a standard.

Peptide Synthesis and Purification. The peptide syntheses were performed at an in-house facility at Florida State University. All peptides were synthesized by solid-phase peptide synthesis using F-moc chemistry protocols. Suitable orthogonal protecting groups were utilized for arginine, glutamine, and aspartic acids. Peptides were cleaved from the resin using 95% trifluroacetic acid (TFA), 2.5% trimethylsilane (TMS), and 2.5% water. Crude peptides were extracted by ether precipitation, purified by use of C-18 reversed-phase chromatography, and characterized by use of matrix-assisted laser desorption ionization mass spectrometry.

NMR Data Collection and Analysis. Protein samples were prepared for NMR in 10 mM potassium phosphate with 10% D_2O, 0.1 mM PMSF, 0.4% EDTA, 0.4% NaN_3, and 0.56 mM 2,2-dimethyl-2-silopentane-5-sulfonate (DSS) as a chemical shift reference. NMR experiments were collected at 30 °C on a 500 MHz Varian Unity *plus* spectrometer equipped with pulsed field gradients and waveform generators by using standard sequences and parameters (*51*) involving gradient coherence selection and sensitivity enhancement in the ^{15}N dimensions. Sweep widths (and number of complex points) were 8333.33 Hz (512), 1650.0 Hz (40), and 7649.9 Hz (64) for ^1H, ^{15}N, and ^{13}C dimensions of the HNCACB, CBCA(CO)NH, and C(CO)NH-TOCSY experiments. A sweep width of 6250 Hz was digitized by 128 or 96 complex points in the indirect proton dimensions of the 3D ^{15}N-separated NOESY-HSQC (100 ms mixing time), 3D ^{13}C-separated HMQC-NOESY (140 ms mixing time), and HCCH-TOCSY (18.6 ms mixing time at 8.7 kH γB_1 field strength) experiments, respectively. An additional 3D ^{15}N-separated NOESY-HSQC spectrum with 140 ms mixing time was collected at 720 MHz using sweep widths that were scaled proportionally to B_0. Assignments for aromatic amino acid side chains were obtained as described previously (*52*). Slowly exchanging hydrogens were identified from a 2D ^1H,^{15}N HSQC spectrum collected 24 h after transferring the sample into 100% D_2O buffer. The backbone torsion angle, ϕ, was determined for residues exhibiting well resolved amide resonances by using the HNHA-J experiment (*53*). All spectra were processed using nmrPipe (*54*) and analyzed using NMRView (*55*) software packages.

Structure Calculations. Interproton distances were estimated from cross-peak intensities in the heteronuclear NOESY experiments. NOE intensities were categorized as strong (1.8−2.8 Å), medium (1.8−3.5 Å), weak (1.8−4.5 Å), or very weak (1.8−5.5 Å) using utilities provided within NMRView. Pseudo atom and proton multiplicity corrections were performed as described (*56*). Hydrogen bond restraints were applied as two distance restraints of 2.4−3.5 and 1.5−2.8 Å for the N−O and H−O internuclear distances, respectively. Backbone ϕ-angles were restrained to −120° ± 30° for residues having $^3J_{HNHA} > 8$ Hz and to −60° ± 30° for residues having $^3J_{HNHA} < 5.4$ Hz. These data, along with Cα and Cβ chemical shifts, were used as input for structure calculations based on a simulated annealing protocol with torsion angle dynamics (*57*) within the CNS package (*58*). Hydrogen bond and dihedral restraints were combined with the NOE restraints in the later stages of structure refinement. A total of 100 initial structures were calculated for SH3 of which 64 showed no restraint violations greater than 0.5 Å and 5°. From these, the 20 lowest energy structures were refined further by Cartesian dynamics with

slow cooling from 300 to 50 K over 10 ps, followed by conjugate gradient energy minimization. The nonbonded interactions were modeled using a modified repulsive potential (*59*). The long loops in Pr−SH3 complicated structure refinement. From a total of 100 initial structures, only 40 showed no restraint violations as above, and of these, the lowest 13 structures were further refined by Cartesian dynamics as above. The lowest energy structures of the two protein constructs were analyzed by using AQUA and PROCHECK software (*60*).

Isothermal Titration Calorimetry. Isothermal titration calorimetry experiments were performed by use of a VP-ITC titration calorimeter (Microcal Inc., Northampton, MA) at 25 °C. Both protein and peptide solutions were dialyzed extensively against 10 mM phosphate buffer, pH 7.5, prior to titration. Protein concentrations were determined from the absoption intensity at 280 nm using a calculated extinction coefficient of 8250 cm^{-1} M^{-1} (www.expasy.ch). Peptide concentrations were determined spectrophotometrically at 257 nm based on a calculated extinction coefficient of 200 cm^{-1} M^{-1}. All titrations were performed with the SH3 domain as titrate (cell) and peptides as titrants (syringe). Depending on the protein concentration, the final protein/peptide molar ratios varied from 1:15 to 1:20, with the corresponding injection volumes of either 5 or 10 μL over 25−30 injections to achieve saturation. Due to the weak intermolecular binding, interpretable isotherms were obtained only at high protein concentrations (∼1.0 mM) with the corresponding peptide concentrations on the order of 15 to 20 mM. Reverse titrations (titrating the SH3 domain into a solution of the peptide) were unsuccessful due to the limited solubility of the SH3 domain in the concentrated stock solution. Blank titrations of peptide into buffer were collected to correct the heats of dilution of the peptides. The heats arising from peptide dilution were fit to a second-order polynomial and then subtracted from the raw protein titration data (*28*, *29*). The corrected binding isotherms were then fit to the standard Wiseman single-site binding equation (*30*) to yield apparent thermodynamic parameters for binding.

Isothermal Equilibrium Denaturation. Changes in protein stability were determined from the change in the intrinsic fluorescence of W104 in the presence of increasing concentration of urea at 25 °C, essentially as described previously (*61*). Samples were prepared at the desired urea concentration and allowed to equilibrate for at least 3 h prior to fluorescence measurements. The concentration of the urea stock solution and the final urea concentration in each sample was determined from the refractive index of the solution (*62*). Fluorescence emission was measured between 290 and 450 nm after excitation at 280 nm in a Cary Eclipse spectrophotometer.

Mutant Generation. Mutations were introduced into the PrSH3 construct using the QuikChange kit (Stratagene, La Jolla, CA) with the Pfu polymerase. The mutant primers 5′-GATGTCAGTCGGTCCGCCTTCGGAAACCC-3′ (P127A), 5′-CCCCTTCGGAAACGCAATTCCAGGTCTC-GAC-3′ (P131A), 5′-CGGAAACCCAATTGCAGGTCTC-GACGAAC-3′ (P133A), and 5′-CAATGGAAAAGATGCC-GAAGCACTCGATGATCTGG-3′ (V211A/L213A double mutant) were used with their complementary strands in the mutagenesis. Positive mutants were identified by PCR screening and direct sequencing of purified plasmid DNA.

NMR Spectroscopy of Mutant PrSH3. 2D ^{1}H,^{15}N-HSQC spectra were collected for the four PrSH3 mutants using spectral conditions identical to those used for wild-type PrSH3 and DtxR (see above). Changes in chemical shift were calculated as (*63*)

$$\Delta\delta = \sqrt{(\Delta\delta_{HN})^2 + (\Delta\delta_N)^2/6.5} \quad (1)$$

Repressor Activity Assay. In vivo assays of repressor activity were performed as described previously (*31*).

ACKNOWLEDGMENT

We thank Donald Caspar for helpful discussions and Dr. Brett Hambly for a careful reading of this manuscript. ITC and CD experiments were performed with partial support of the Physical Biochemistry Facility in the Kasha Laboratory.

SUPPORTING INFORMATION AVAILABLE

Single composite figure of three 2D ^{1}H, ^{15}N HSQC spectra collected on PrSH3 at 1 mM (black contours), 500 μM (magenta contours), and 100 μM (blue contours). This material is available free of charge via the Internet at http://pubs.acs.org.

REFERENCES

1. Jakubovics, N. S., and Jenkinson, H. F. (2001) Out of the iron age: new insights into the critical role of manganese homeostasis in bacteria, *Microbiology 147*, 1709−1718.
2. Tao, X., Schiering, N., Zeng, H.-Y., Ringe, D., and Murphy, J. R. (1994) Iron, DtxR, and the regulation of diphtheria toxin expression, *Mol. Microbiol. 14*, 191−197.
3. Boyd, J., Oza, M. N., and Murphy, J. R. (1990) Molecular cloning and DNA sequence analysis of a diptheria *tox* iron-dependent regulatory element (*dtxR*) from *Cornybacterium diptheriae*, *Proc. Natl. Acad. Sci. U.S.A. 87*, 5968−5972.
4. Lee, J. H., and Holmes, R. K. (2000) Characterization of specific nucleotide substitutions in DtxR-specific operators of *Corynebacterium diphtheriae* that dramatically affect DtxR binding, operator function, and promoter strength, *J. Bacteriol. 182*, 432−438.
5. Schmitt, M. P. (1997) Transcription of the *Corynebacterium diphtheriae humO* gene is regulated by iron and heme, *Infect. Immun. 65*, 4634−4641.
6. Braun, V., and Killmann, H. (1999) Bacterial solutions to the iron-supply problem, *Trends. Biochem. Sci. 24*, 104−109.
7. Braun, V. (2001) Iron uptake mechanisms and their regulation in pathogenic bacteria, *Int. J. Med. Microbiol. 291*, 67−79.
8. Ratledge, C., and Dover, L. G. (2000) Iron metabolism in pathogenic bacteria, *Annu. Rev. Microbiol. 54*, 881−941.
9. Schiering, N., Tao, X., Zeng, H., Murphy, J. R., Petsko, G. A., and Ringe, D. (1995) Structures of the apo- and metal ion-activated forms of the diphtheria *tox* repressor from *Corynebacterium diphtheriae*, *Proc. Natl. Acad. Sci. U.S.A. 92*, 9843−9850.
10. Qiu, X., Verlinde, C. L. M. J., Zhang, S., Schmitt, M. P., Holmes, R. K., and Hol, W. G. J. (1995) Three-dimensional structure of the diphtheria toxin repressor in complex with divalent cation co-repressors, *Structure 3*, 87−100.
11. Qiu, X., Pohl, E., Holmes, R. K., and Hol, W. G. J. (1996) High-resolution structure of the diptheria toxin repressor complexed with cobalt and manganese reveals an SH3-like third domain and suggests a possible role of phosphate as co-corepressor, *Biochemistry 35*, 12292−12302.
12. Pohl, E., Holmes, R. K., and Hol, W. G. J. (1999) Crystal structure of a cobalt-activated diphtheria toxin repressor-DNA complex reveals a metal-binding SH3-like domain, *J. Mol. Biol. 292*, 653−667.
13. Wang, G., Wylie, G. P., Twigg, P. D., Caspar, D. L. D., Murphy, J. R., and Logan, T. M. (1999) Solution structure and peptide binding studies of the C-terminal Src homology 3-like domain of the diphtheria toxin repressor protein, *Proc. Natl. Acad. Sci., U.S.A. 96*, 6119−6124.

14. Tao, X., and Murphy, J. R. (1992) Binding of the metaolloregulatory protein DtxR to the Diptheria *tox* operator requires divalent heavy metal ion and protects the palindromic sequence from DNase I digestion, *J. Biol. Chem. 267*, 21761−21764.
15. Ding, X., Zeng, H., Schiering, N., Ringe, D., and Murphy, J. R. (1996) Identification of the primary metal ion-activation sites of the diphtheria tox repressor by X-ray crystallography and site-directed mutagenesis, *Nat. Struct. Biol. 3*, 382−387.
16. Pohl, E., Holmes, R. K., and Hol, W. G. (1999) Crystal structure of the iron-dependent regulator (IdeR) from *Mycobacterium tuberculosis* shows both metal binding sites fully occupied, *J. Mol. Biol. 285*, 1145−1156.
17. Love, J. F., VanderSpek, J. C., and Murphy, J. R. (2003) The src homology 3-like domain of the diphtheria toxin repressor (DtxR) modulates repressor activation through interaction with the ancillary metal ion-binding site, *J. Bacteriol. 185*, 2251−2258.
18. Twigg, P. D., Parthasarathy, G., Guerrero, L., Logan, T. M., and Caspar, D. L. (2001) Disordered to ordered folding in the regulation of diphtheria toxin repressor activity, *Proc. Natl. Acad. Sci. U.S.A. 98*, 11259−11264.
19. Spiering, M. M., Ringe, D., Murphy, J. R., and Marletta, M. A. (2003) Metal stoichiometry and functional studies of the diphtheria toxin repressor, *Proc. Natl. Acad. Sci. U.S.A. 100*, 3808−3813.
20. Xu, W., Harrison, S. C., and Eck, M. L. (1997) Three-dimensional structure of the tyrosine kinase c-Src, *Nature 385*, 595−602.
21. Sicheri, F., Maorefi, I., and Kuriyan, J. (1997) Crystal structure of the Src family tyrosine kinase Hck, *Nature 385*, 602−609.
22. Wider, C., Weber, C., Traber, R., Widmer, H., and Wüthrich, K. (1990) Use of a double-half- filter in two-dimensional ^{1}H nuclear magnetic resonance studies of receptor-bound cyclosporin, *J. Am. Chem. Soc. 112*, 9015−9016.
23. Wu, D., Chen, A., and C. S. Johnson, J. (1995) An improved diffusion-ordered spectroscopy experiment incorporating bipolar-gradient pulses, *J. Magn. Reson. A115*, 260−264.
24. Stapley, B. J., and Creamer, T. P. (1999) A survey of left-handed polyproline II helices, *Protein Sci. 8*, 587−595.
25. Kuriyan, J., and Cowburn, D. (1997) Modular peptide recognition domains in eukaryotic signaling, *Annu. Rev. Biophys. Biomol. Struct. 26*, 259−288.
26. Reed, J., and Kinzel, V. (1991) A conformational switch is associated with receptor affinity in peptides derived from the CD4-binding domain of gp120 from HIV I, *Biochemistry 30*, 4521−4528.
27. Fukada, H., and Takahashi, K. (1998) Enthalpy and heat capacity changes for the proton dissociation of various buffer components in 0.1 M potassium chloride, *Proteins 33*, 159−166.
28. Parker, M. H., Brouillette, C. G., and Prevelige, P. E., Jr. (2001) Kinetic and calorimetric evidence for two distinct scaffolding protein binding populations within the bacteriophage P22 procapsid, *Biochemistry 40*, 8962−8970.
29. Graversen, J. H., Sigurskjold, B. W., Thogersen, H. C., and Etzerodt, M. (2000) Tetranectin-binding site on plasminogen kringle 4 involves the lysine-binding pocket and at least one additional amino acid residue, *Biochemistry 39*, 7414−7419.
30. Wiseman, T., Williston, S., Brandts, J. F., and Lin, L.-N. (1989) Rapid measurement of binding constants and heats of binding using a new titration calorimeter. *Anal. Biochem. 179*, 131−137.
31. Love, J. F., and Murphy, J. R. (2002) Design and development of a novel genetic probe for the analysis of repressor-operator interactions, *J. Microbiol. Methods 51*, 63−72.
32. Saraste, M., and Musacchio, A. (1994) Backwards and forwards binding, *Nat. Struct. Biol. 1*, 835−837.
33. Kay, B. K., Williamson, M. P., and Sudol, M. (2000) The importance of being proline: the interaction of proline-rich motifs in signaling proteins with their cognate domains, *FASEB J. 14*, 231−241.
34. Kang, H., Freund, C., Duke-Cohan, J. S., Musacchio, A., Wagner, G., and Rudd, C. E. (2000) SH3 domain recognition of a proline-independent tyrosine-based RKxxYxxY motif in immune cell adaptor SKAP55, *EMBO J. 19*, 2889−2899.
35. Kami, K., Takeya, R., Sumimoto, H., and Kohda, D. (2002) Diverse recognition of non-PxxP peptide ligands by the SH3 domains from p67(phox), Grb2 and Pex13p, *EMBO J. 21*, 4268−4276.
36. Gorina, S., and Pavletich, N. P. (1996) Structure of the p53 tumor suppressor bound to the ankyrin and SH3 domains of 53bp2, *Science 274*, 1001−1005.
37. Berry, D. M., Nash, P., Liu, S. K., Pawson, T., and McGlade, C. J. (2002) A high-affinity Arg-X-X-Lys SH3 binding motif confers specificity for the interaction between Gads and SLP-76 in T cell signaling, *Curr. Biol. 12*, 1336−1341.
38. Brazin, K. N., Fulton, D. B., and Andreotti, A. H. (2000) A specific intermolecular association between the regulatory domains of a Tec family kinase, *J. Mol. Biol. 302*, 607−623.
39. Stock, A. M., Robinson, V. L., and Goudreau, P. N. (2000) Two-component signal transduction, *Annu. Rev. Biochem. 69*, 183−215.
40. Ponting, C. P., Aravind, L., Schultz, J., Bork, P., and Koonin, E. V. (1999) Eukaryotic signalling domain homologues in archaea and bacteria. Ancient ancestry and horizontal gene transfer, *J. Mol. Biol. 289*, 729−745.
41. Whisstock, J. C., and Lesk, A. M. (1999) SH3 domains in prokaryotes, *Trends. Biochem. Sci. 24*, 132−133.
42. Ferreon, J. C., and Hilser, V. J. (2003) Ligand-induced changes in dynamics in the RT loop of the C-terminal SH3 domain of Sem-5 indicate cooperative conformational coupling, *Protein Sci. 12*, 982−996.
43. Paras-Lutzke, R. A., Vink, C., and Plasternak, R. H. A. (1994) Characterization of the minimal DNA-binding domain of the HIV integrase protein, *Nucl. Acids Res. 22*, 4125−4131.
44. Wittekind, M., Mapelli, C., Farmer, B. T, II, Suen, K.-L., Goldfarb, V., Tsao, J., Lavoie, T., Barbacid, M., Meyers, C. A., and Mueller, L. (1994) Orientation of peptide fragments from Sos protein bound to the N-terminal SH3 domain of Grb2 determined by NMR spectroscopy, *Biochemistry 33*, 13531−13539.
45. Petrella, E. C., Machesky, L. M., Kaiser, D. A., and Pollard, T. D. (1996) Structural requirements and thermodynamics of the interaction of proline peptides with profilin, *Biochemistry 35*, 16535−16543.
46. Makhatadze, G. I., and Privalov, P. L. (1994) Energetics of interactions of aromatic hydrocarbons with water, *Biophys. Chem. 50*, 285−291.
47. Ferreon, J. C., and Hilser, V. J. (2004) Thermodynamics of binding to SH3 domains: The energetic impact of polyproline II (P_{II}) helix formation, *Biochemistry 43*, 7787−7797.
48. Zhou, H.-X. (2001) Loops in proteins can be modeled as worm-like chains, *J. Phys. Chem. B 105*, 6763−6736.
49. Goranson-Siekierke, J., Pohl, E., Hol, W. J. G., and Holmes, R. K. (1999) Anion-coordinating residues at binding site 1 are essential for the biological activity of the diphtheria toxin repressor, *Infect. Immun. 67*, 1806−1811.
50. Hantke, K. (2001) Iron and metal regulation in bacteria, *Curr. Opin. Microbiol. 4*, 172−177.
51. Muhandiram, D. R., and Kay, L. E. (1994) Gradient-enhanced triple-resonance three-dimensional NMR experiments with improved sensitivity, *J. Magn. Reson. 103B*, 203−216.
52. Twigg, P. D., Wylie, G. P., Wang, G., Murphy, J. R., Caspar, D. L. D., and Logan, T. M. (1999) Expression and assignment of the ^{1}H, ^{15}N, and ^{13}C resonances of the C-terminal domain of diphtheria toxin repressor, *J. Biomol. NMR 13*, 197−198.
53. Kuboniwa, H., Grzesiek, S., Delagio, F., and Bax, A. (1994) Measurement of Hn-Ha J couplings in calcium-free calmodulin using new 2D and 3D water flip-back methods, *J. Biomol. NMR 4*, 871−878.
54. Delaglio, F., Grzesiek, S., Vuister, G. W., Zhu, G., Pfeifer, J., and Bax, A. (1995) NMRPipe: A multidimensional spectra processing system based on UNIX pipes, *J. Biomol. NMR 6*, 277−293.
55. Johnson, B. A., and Blevins, R. A. (1994) NMRView: A computer program for the visualization and analysis of NMR data, *J. Biomol. NMR 4*, 603−614.
56. Fletcher, C. M., Jones, D. N. M., Diamond, R., and Neuhaus, D. (1996) Treatment of NOE constraints involving equivalent or nonstereoassigned protons in calculations of biomacromolecular structures, *J. Biomol. NMR 8*, 292−310.
57. Stein, E. G., Rice, L. M., and Brünger, A. T. (1997) Torsion-angle molecular dynamics as a new efficient tool for NMR structure calculation, *J. Magn. Reson. 124*, 154−164.
58. Brunger, A. T., Adams, P. D., Clore, G. M., DeLano, W. L., Gros, P., Grosse-Kunstleve, R. W., Jiang, J. S., Kuszewski, J., Nilges, M., Pannu, N. S., Read, R. J., Rice, L. M., Simonson, T., and Warren, G. L. (1998) Crystallography & NMR system: A new software suite for macromolecular structure determination, *Acta Crystallogr. D Biol. Crystallogr. 54*, 905−921.

59. Linge, J. P., and Nilges, M. (1999) Influence of nonbonded parameters on the quality of NMR structures: a new force field for NMR structure calculation, *J. Biomol. NMR 13*, 51−59.
60. Laskowski, R. A., Rullmann, J. A. C., MacArthur, M. W., Kaptein, R., and Thornton, J. M. (1996) AQUA and PROCHECK-NMR: Programs for checking the quality of protein structuers solved by NMR, *J. Biomol. NMR. 8*, 477−486.
61. Korepanova, A., Douglas, C., and Logan, T. M. (2002) Glutamine 53 is a gatekeeper residue in the FK506 binding protein, *J. Mol. Biol. 323*, 285−296.
62. Mulder, F. A. A., Schipper, D., Bott, R., and Boelens, R. (1999) Altered flexibility in the substrate-binding site of related native and engineered high-alkaline Bacillus subtilisins, *J. Mol. Biol. 292*, 111−123.
63. Eldridge, A. M., Kang, H. S., Johnson, E., Gunsalus, R., and Dahlquist, F. W. (2002) Effect of phosphorylation on the interdomain interaction of the response regulator, NarL, *Biochemistry 41*, 15173−15180.
64. Koradi, R., Billeter, M., and Wüthrich, K. (1996) MOLMOL: A program for display and analysis of macromolecular structures, *J. Mol. Graphics 14*, 51−55.

BI048035P